Open Access

Accepted Uncorrected Research Article†

PRNANO

Precis. Nanomed. 6(1):994-1006, 2023

ANDOVER HOUSE

Polymeric nanocarriers co-encapsulating PET probes and protein therapeutics

Chester E. Markwalter[1a], Leon Z. Wang[1], Ola M Sharaf[2], Prashanth Padakanti[2], Mark Esposito[3], Brian K. Wilson[1], Eric Blankemeyer[2], Sean D. Carlin[2], Abass Alavi[2], Robert K. Prud'homme[1]*

1 Dept of Chemical and Biological Engineering, Princeton University, Princeton, NJ.
2 Dept of Radiology, Perelman School of Medicine, University of Pennsylvania, Philadelphia, PA
3 Optimeos Life Sciences, 174 Nassau St Princeton NJ
a Current address: Optimeos Life Sciences, 174 Nassau St Princeton, NJ, 08542.
Email: cmarkwalter@optimeos.com

Submitted: September 29, 2022 Accepted: December 8, 2022 Prelim. Published: December 13, 2022

Graphical Abstract

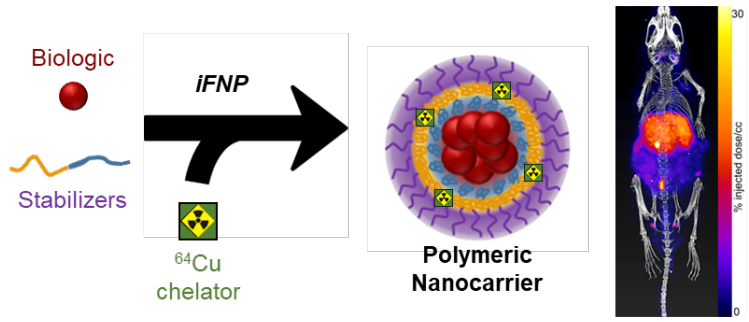

Abstract:

Nanocarriers encapsulating nucleic acids or protein therapeutics are important tools for modulating biodistribution and enhancing the intracellular delivery of biologics. We have recently developed inverse Flash NanoPrecipitation (iFNP), demonstrating its effectiveness in encapsulating biologics at high loadings and encapsulation efficiency. Here, we present the biodistribution of two iFNP nanocarriers using ^{64}Cu positron emission tomography imaging in a murine adenocarcinoma xenograft model characterized by elevated macrophage content. Two nanocarriers with similar sizes and surfaces were prepared. iFNP produces core-shell-corona nanocarriers where the hydrophobic shell layer in one case was poly(lactic acid) (PLA), and the other nanocarrier shell was poly(styrene) (PS). While the expectation was that the biodistribution and clearance of both nanocarriers would be similar, it was found that the clearance of the PS nanocarrier occurred in less than 3 hours while the PLA nanocarrier exhibited sustained circulation times. The mechanism of nanocarrier instability for the PS shell nanocarrier manifests as the development of a negative surface charge due to the exposure of the anionic nanocarrier inner core. The stable PLA-based formulation exhibited circulation times greater than 24 hours and enhanced accumulation in the lymphatics and the tumor relative to the unstable formulation. The novel mechanism of encapsulation by iFNP motivates the fundamental studies on nanoparticle biodistribution reported here.

Keywords:

Nanoparticle, macrophage, PET imaging, biologics, proteins, nanocarrier, polylactic acid, PLA, Flash NanoPrecipitation

---

†This is a PDF file of an article that has undergone copyediting, typesetting, and formatting, but it is not yet the definitive version of record. This version will undergo additional review before its final version is published. Please note that during that process, errors may be discovered, which could affect the content.

*Corresponding author: A301 Engineering Quad, Olden St., Princeton, NJ, 08544. Email: prudhomm@princeton.edu

Rationale, Purpose, and Limitations

This study provides design insight for nanoformulations encapsulating biologics and further clarity into key parameters impacting nano-bio interactions through a ^{64}Cu-enabled positron emission tomography (PET) study of nanocarrier biodistributions in a mouse model. We employ a nanocarrier assembly method, inverse Flash NanoPrecipitation (iFNP), that allows for the encapsulation of peptides, proteins, and nucleic acids in the core and a hydrophobic copper chelator in the nanocarrier shell. Although, the unexpected instability mechanism we describe is characterized only for nanocarriers produced by iFNP, the approach is broadly applicable to all nanocarriers.

Introduction

The inverse Flash NanoPrecipitation (iFNP) process encapsulates peptides, proteins, and nucleic acids by an insolubility-driven precipitation process that does not use charge complexation to drive nanocarrier (NC) formation.[1-7] It employs two sequential block copolymer-directed assembly steps to first encapsulate the biologic and then install a surface coating such as poly(ethylene glycol) (PEG), as detailed schematically in Figure 1A. The initial encapsulation step occurs in a non-polar organic solvent phase, and the coating step transitions the NC into an aqueous system. This approach results in higher loadings than are possible by liposome or polymersome encapsulation. The sequential nature of the process also provides an opportunity for co-encapsulation of hydrophobic species into the hydrophobic shell that forms during the coating step. The iFNP technique extends the Flash NanoPrecipitation (FNP) process, which uses specialized mixers to assemble nanoparticles at high flow rates.[8-11] Consequently, it is highly translatable from bench to clinical scale.[12]

Imaging the biodistribution and fate of NCs is essential to therapeutic development. PET imaging is especially powerful *in vivo* imaging modality. The radionuclide ^{64}Cu is a PET agent suited for fate and PK studies due to its 12.7-hour half-life. Previously, facile post-assembly loading of ^{64}Cu into solid-core NCs assembled by FNP had been enabled by incorporating a small molecule hydrophobic phthalocyanine dye as copper chelator into the hydrophobic core of the nanoparticle (Figure 1B).[13,14] This contrasts with conventional approaches of using large complexing ligands (DOTA or DFO) on the surface of the NC.[15,16] Our concern is that these surface-bound ligands may create specific biological interactions that bias the biodistribution.

The sequential polymer assembly steps used in iFNP enable co-encapsulation of water-soluble therapeutics in the core and hydrophobic compounds in the shell in a decoupled manner. Here, we co-encapsulate into the hydrophobic polymer shell a small molecule hydrophobic phthalocyanine dye ('762) that enables post-assembly chelation of PET-active ^{64}Cu in iFNP (Figure 1B).[14]

Experimental Design

Our hypothesis was that the NC surface (corona) determines the interactions of the NC with the biological milieu *in vivo* and that two NCs with the same surface properties would have similar *in vivo* fates, independent of the composition of the core. Therefore, two iFNP constructs were made with the same 5kDa PEG surface but comprising two different hydrophobic shells: polystyrene (PS-iFNP-NC) and polylactic acid (PLA-iFNP-NC). We used poly(styrene)-*b*-poly(acrylic acid) (PS-*b*-PAA) or poly(lactic acid)-*b*-poly(aspartic acid) (PLA-*b*-PAsp), respectively, to form the shell of these NCs. After assembly, the polyacid block in the NC core was ionically crosslinked with iron or calcium to stabilize the NC for the coating step.

Contrary to our hypothesis, we observed significant differences *in vivo* between PS and PLA formulations. We identified the mechanism whereby, for the PS shell containing the copper chelator, an instability exposes the negatively charged polyacid in the core, resulting in a negatively charged coated NC. This instability does not occur in the absence of the chelator. The long circulation times seen for the PLA-iFNP-NCs indicate their suitability for encapsulation and delivery of biologics. Whereas the negatively charged PS NCs are cleared rapidly, as is observed for other negatively charged NCs.[17-19] These findings provide design insight for nanoformulations and further clarity into key parameters impacting nano-bio interactions.

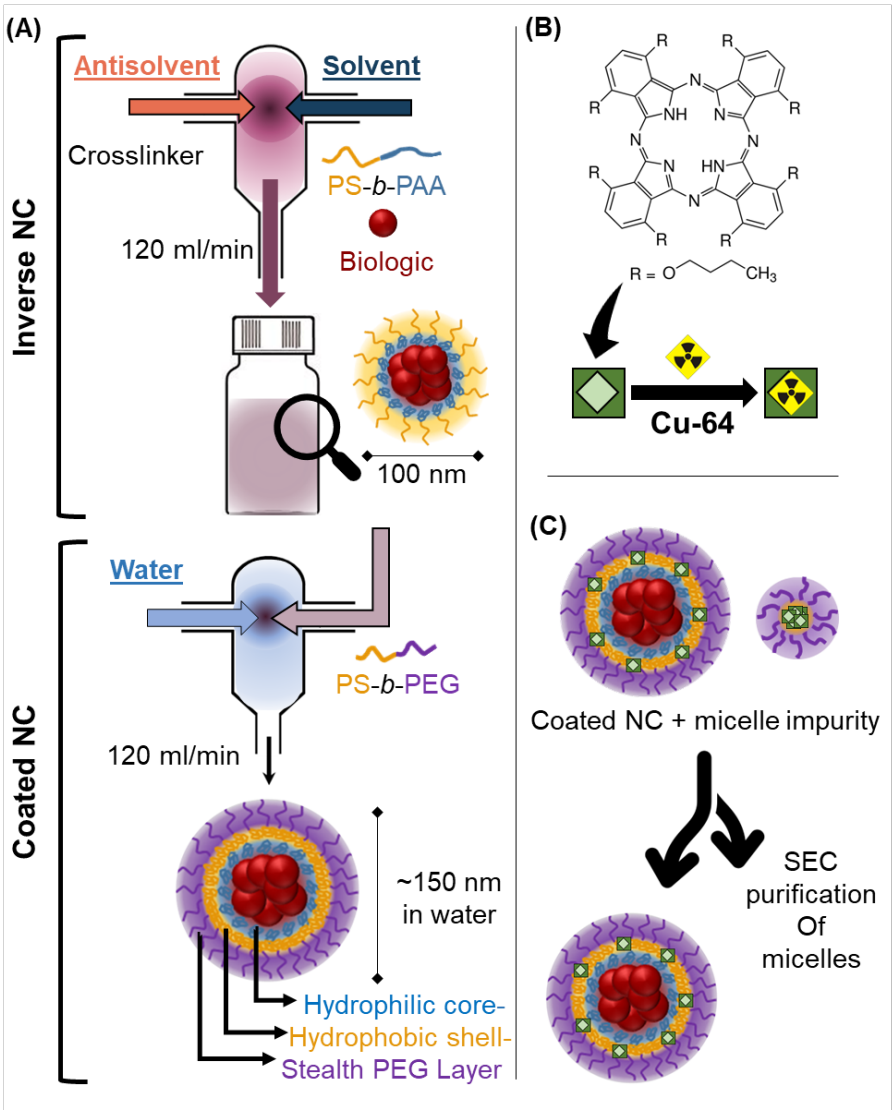

Figure 1: (A) Process flow diagram for inverse Flash NanoPrecipitation (iFNP) showing the two assembly steps in the process to form inverse NCs followed by coated NCs. An extraction and solvent exchange to a miscible solvent such as tetrahydrofuran is omitted for clarity before the coating step. (B) Positron emission tomography studies used a radionuclide, ^{64}Cu, chelated by a phthalocyanine derivative that had been incorporated into the NC. (C) The hydrophobic chelator was incorporated during the coating step. Sequestration of chelator into a micelle population was mitigated through purification using size exclusion chromatography (SEC).

Materials and Methods

Materials

1,4,8,11,15,18,22,25-octabutoxy-29H,31H-phthalocyanine ('762 - the designation of the copper chelator), Drabkin's Reagent, α-tocopherol acetate, ethylenediaminetetraacetic acid (EDTA), bovine serum albumin (fatty acid-free, low endotoxin, >96%), maltodextrin DE4-7, sodium acetate, copper (II) sulfate, RPMI-1640 and lysozyme from chicken egg white (>90%) were purchased from Sigma-Aldrich (St. Louis, MO). Sodium chloride (ACS grade), AlexaFluor-488 5-SDP ester, trifluoroacetic acid (peptide synthesis grade), dimethyl sulfoxide (HPLC grade), methanol (HPLC grade), methylene chloride (ACS grade), and tetrahydrofuran (HPLC grade) were purchased from Thermo Fisher Scientific (Waltham, MA). $PLA_{4.2k}$-*b*-$mPEG_{5k}$ was a gift from Evonik (Essen, Germany). BioWhittaker® phosphate-buffered saline (without calcium or magnesium) was purchased from Lonza (Basel, Switzerland). Dulbecco's modified Eagle's medium (DMEM), fetal bovine serum, and glutamax was purchased from Gibco (Paisley,

UK). Deionized water (MQ) (18.2 MΩ·cm) was generated by a NANOpure Diamond UV ultrapure water system (Barnstead International, Germany). Poly(acrylic acid)-*b*-poly(styrene) (4.8k-*b*-5k PDI 1.4, 4.3k-*b*-15k PDI 1.15, and 5.5k-*b*-52k PDI 1.08) and $PS_{1.6k}$-*b*-PEG_{5k} was purchased from Polymer Source (Dorval, Quebec). $PAsp_{5k}$-*b*-PLA_{10k}-*b*-$PAsp_{5k}$ (PLA_{5k}), $PAsp_{5k}$-*b*-PLA_{40k}-*b*-$PAsp_{5k}$ (PLA_{20k}), and $PAsp_{2k}$-*b*-PLA_{15k} were kindly provided by R. Pagels of Optimeos.

Procedure for iFNP-NC Formation

iFNP-NCs were prepared using previously described techniques that involve inverse NC formation (iFNP step), DMSO extraction, solvent exchange, and coating of the inverse NC with the second block copolymer (coating step).[2,6] If coated using a confined impinging jet (CIJ) mixer, the inverse NCs were combined with '762 and the polymer stabilizer ($PS_{1.6k}$-*b*-PEG_{5k} or $PLA_{4.2k}$-b-PEG_{5k}) in tetrahydrofuran (THF) at a target mass ratio. This solution was then rapidly mixed against an equal volume of water and collected in a vial containing additional water. Formulations requiring a multi-inlet vortex mixer (MIVM) were prepared as above except the polymer was segregated into a separate THF stream with concentrations as indicated.

The PS-iFNP-NC for *in vivo* studies was produced in an MIVM. The first stream was composed of DMSO with 5 vol% water and 5 mg/ml lysozyme. The second stream was THF with 15 mg/ml of PS_{52k}-*b*-$PAA_{5.5k}$. The remaining two streams were chloroform, each of which contained 5 vol% of a methanol solution of the iron crosslinker. The extraction was done twice to ensure the complete removal of DMSO and unbound iron crosslinker. The coating step was carried out in a MIVM. The first THF stream contained the inverse NCs at 10.2 mg/ml, '762 at 2.7 mg/ml, and α-tocopherol acetate (0.9 mg/mL). The second THF stream contained $PS_{1.6k}$-*b*-PEG_{5k} at 30 mg/ml. The remaining streams were deionized water.

The PLA-iFNP-NC for *in vivo* studies was prepared in a CIJ with a DMSO stream containing 10 v% water, 5 mg/ml maltodextrin DE4-7, and 15 mg/ml $PAsp_{2k}$-*b*-PLA_{15k}. The antisolvent stream was chloroform containing 1 charge equivalent of calcium crosslinker. The coating was carried out in the MIVM. The $PLA_{4.2k}$-b-PEG_{5k} solution was added in one stream at a 3:1 mass ratio of block copolymer to inverse NC. The '762 dye was added to the inverse NC stream at 1:4 ratio relative to the inverse NC. The other two streams were deionized water.

The CIJ and MIVM mixers are available from Holland Applied Technologies, Burr Ridge, IL.

Dynamic Light Scattering Analysis

Particle size was characterized by Dynamic Light Scattering (DLS) using a Zetasizer Nano ZS (Malvern, Worcestershire, UK) at 25°C. Size distributions were determined from a CONTIN analysis implemented by the Zetasizer software. Zeta potential (surface charge) was measured using a diluent of 0.1× phosphate-buffered saline (~20 mM total ionic strength).

Stability studies were conducted in an orbital shaker at 37°C on iFNP-NCs dispersed in the specified buffer. Aliquots were sampled at the indicated time and diluted for DLS and zeta potential measurement.

SEC Purification Protocol

A coated iFNP-NC dispersion was concentrated and filtered (0.45 μm) and then injected onto a HiPrep Sephacryl S-500 size exclusion column (GE Healthcare, Chicago, IL) at room temperature. The mobile phase was 150 mM NaCl solution. The desired fractions were pooled and concentrated by ultrafiltration. For *in vivo* studies, mass concentration was determined by thermogravimetric analysis.[1]

Copper Loading

The purified iFNP-NC was mixed with a 300 mM acetate buffer (pH 5.5), at a 6:4 volume ratio. Copper (II) sulfate in deionized water was added to the desired mole ratio (typically 10×), or for *in vivo* studies, 111 MBq of ^{64}Cu (II) Chloride. Previous studies have shown no significant differences between Cu(II) chloride and sulfate salts for loading.[13,14] The NCs were incubated for 3 hours at 37°C and then washed on a 100 kDa ultrafilter with isotonic acetate buffer (pH 6.5). Loading was confirmed by UV-VIS analysis of the iFNP-NC dispersion diluted in THF or by activity measurement.

Biodistribution study

Mouse tumor model.

All animal studies were conducted per University of Pennsylvania IACUC regulations and guidelines. Tumors were initiated in 6–8-week-old male C57BL/6J mice by subcutaneous flank inoculation of 5 X 10^6 152.PDA in 50 µl PBS plus 50 µL of matrigel. Tumors were allowed to develop and routinely used for imaging studies on day 16 post-inoculation, with a volume of approximately 500 mm^3.

PET-CT imaging.

Three mice per arm were administered between 150 and 250 µCi of ^{64}Cu-labelled NCs in a bolus volume of approximately 100 µL via tail-vein injection. After a distribution period of 3 hours, mice were anesthetized by isoflurane inhalation (2% for induction, 1.5% for maintenance) and placed on a heated animal bed. Three hours post-injection, PET images were acquired on a Molecubes X-cube small animal PET scanner for 30 minutes continuously in list mode. The animals were then transferred to a Molecubes X-cube small animal computed tomography (CT) scanner, and CT images acquired in 'high quality' mode. Animals were then returned to cages and allowed to recover fully. The animals were imaged serially at 6- and 24-hours post-injection using an identical protocol. Images were reconstructed using the manufacturer's interactive reconstruction algorithms, and co-registered using on-board 3-D spatial mapping algorithms. Region of Interest analysis of tumor and target organs was performed using VivoQuant 4.0 software.

Ex vivo histology and imaging.

Following PET imaging, tumors were excised, embedded in OCT mounting medium and snap-frozen. Contiguous 10µm sections were cut and stored at −80ºC until used. For digital autoradiographic determination of ^{64}Cu distribution, tissue sections were exposed to a phosphor plate (BAS-IP SR2040) for 48 hours, and images were acquired using a GE Typhoon 7000 plate reader. The same tissue sections were then stained with H&E. Sequential sections were manually stained for the mouse macrophage marker F4/80, using the rat monoclonal antibody A3-1 (Invitrogen). Secondary detection was carried out using a biotinylated goat anti-rat secondary (Invitrogen), and a signal was developed using a Vectastain ABC-HRP kit (Vector laboratories). Brightfield microscopic images of the entire tumor section were obtained using a Zeiss AxioImager2 scanning microscope fitted with a ×10 objective and motorized stage. As a final step, all digital image datasets were registered using ImageJ.

Hemolysis Assay

We employed the Nanotechnology Characterization Laboratory ITA-1 (National Laboratory for Cancer Research) method. Rat whole blood was collected under Princeton University protocol #2134A-19. FNP-NC and iFNP-NCs were prepared using standard methods and washed to remove residual solvent.

Rat whole blood was diluted in PBS to 10 mg/mL total hemoglobin. Hemolysis samples were prepared by mixing 100 µL of NC dispersion with 700 µL of PBS and 100 µL of diluted whole blood. The samples were incubated at 37°C for 3 hours, inverted every 30 minutes to keep cells suspended. All samples were centrifuged for 15 minutes at 800 RCF. The supernatant was diluted 50% with Drabkin's Reagent and analyzed at 540 nm.

Fluorescent iFNP-NC production

Alexa Fluor 488 was added in DMSO (0.5 mg at 10 mg/ml) to a micelle dispersion of the PAsp-*b*-PLA block copolymer in sodium bicarbonate buffer (100 mM, pH 7.8). After 1 hour of stirring at room temperature, the micelles were extensively buffer exchanged on a 100 kDa ultrafilter to deionized water. Trifluoracetic acid (5 equivalents concerning the PAsp sidechains) was added to generate the free acid form of the PAsp side chains and form a fluorescent pellet, which was further washed with water. The purified block copolymer was then lyophilized and used for iFNP.

Cell Culture

Cell lines used were HepG2 (ATCC), Tib-67 (ATCC; also known as J774A.1), HEK293T (ATCC), and 152.PDA murine pancreatic adenocarcinoma, kindly gifted by the laboratory of Gregory Beattie, University of Pennsylvania, derived from a pancreatic ductal adenocarcinoma tumor arising spontaneously in genetically-modified KPC mice, and was selected for this study due to the observation of high prevalence of tumor-infiltrating macrophages.[20] HepG2, Tib-67, and HEK293T were grown in

DMEM supplemented with 10% fetal bovine serum, 152. PDA were grown in DMEM with 10% fetal calf serum supplemented with L-glutamine. All cultures used 100 units/mL of penicillin, 100 µg/mL of streptomycin, and 0.25 µg/mL of Amphotericin B. Cells were grown in a humidified incubator with 5% CO^2 atmosphere, and were tested for mycoplasma contamination every 8 weeks. STR profiling was not performed due to the direct receipt of human cell lines from ATCC.

Cell Uptake Studies

FNP-NCs with PEG or PAsp coating were prepared for the hemolysis assay, adding DiO fluorescent dye at 0.5 wt% as a fluorescent tracer. The iFNP-NCs were prepared using the fluorescent PAsp-*b*-PLA. Inverse NCs encapsulating bovine serum albumin (BSA) modified with Alexa Fluor 488 were prepared in an MIVM. One stream contained 8 mg/mL of BSA in DMSO containing 16% MQ. The second stream contained 12 mg/mL of PAsp-*b*-PLA. The third stream contained THF as an antisolvent. The fourth stream contained $CHCl_3$ at a 4-fold higher volume ratio. The formulations were calcium crosslinked by adding the solution in methanol after inverse NC assembly.

For cell uptake studies, nanoparticles were added to adherent cell cultures with a starting confluence of 30-50% and were incubated for 24 hours at standard cell culture conditions. Short-term cell binding studies were performed by trypsinizing cells, washing once with PBS, and resuspending cells in PBS at room temperature, followed by adding nanoparticles for ten minutes with vortexing every two minutes. Next, cells were washed and resuspended in PBS + 500 ng/mL DAPI followed by analysis using the Attune NxT flow cytometer (ThermoFisher). Singlet cells were gated using SSC-A × SSC-H, and live cells were gated from the DAPI-negative population. Fluorescent intensity was captured on the BL-1 channel without compensation. Baseline correction was performed by subtracting MFI of cells exposed to DAPI only.

Results

Biodistribution studies reveal the different fate of PS and PLA nanocarriers

iFNP-NCs were produced using PS-based or PLA-based stabilizers and then purified by size exclusion chromatography to remove PEG micelles present after coating (SI Figures S1-S5). NCs were characterized by DLS and found to be similar in size and surface charge (Table 1). They were spherical in shape by TEM imaging (SI Figure S16). The model biologic for PS-iFNP-NCs was lysozyme, and for PLA-iFNP-NCs was dextran. The different cores were implemented to produce similarly sized NCs. Previous reports describe these formulations' encapsulation efficiency and release behavior in detail.[6,7] We used UV-VIS, EDTA challenge, and radiometric measurements to confirm the chelation of copper by the '762 dye with >95% efficiency (SI Figures S7-S9).

Table 1: DLS characterization of in vivo nanocarrier formulation size and zeta potential (ζ). Average and standard deviation is of triplicate preparations. Size is the intensity-weighted distribution analysis.

	Size, nm	**ζ, mV**	**PDI**
PS-iFNP-NC	155±6	−5.5±2.1	0.13±0.01
PLA-iFNP-NC	120±7	−5.0±0.6	0.13±0.01

We administered iFNP-NCs at 150-250 µCi per animal by tail vein injection and imaged at 3 hours, 6 hours, and 24 hours (Figure 2). PS-iFNP-NCs unexpectedly exhibited terminal biodistributions distinct from that of PLA-iFNP-NC. The PS-iFNP-NC clearance to the liver and spleen was nearly complete by the initial 3-hour imaging time point with minimal change observed subsequently. PLA-iFNP-NC clearance to the liver and spleen was slower with broader systemic exposure persisting even at 24 hours. Maximum intensity projections further support this finding (Figure 3A). The PLA-iFNP-NC formulation was found to accumulate in multiple lymph nodes, including both the cervical and abdominal lymph. This accumulation in secondary lymphoid organs is notable for potential immunological applications.

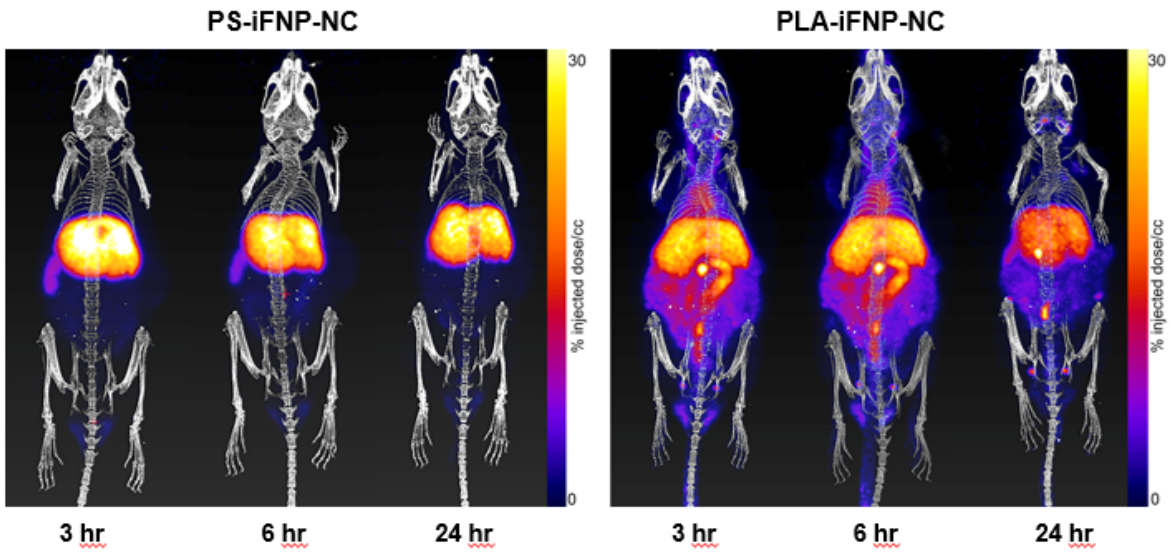

Figure 2: Whole animal images taken at the indicated time point for the specified formulation. Each animal was representative of the cohort. Heat map colors indicate %ID/cc.

Based on NC size analysis, we expect that accumulation was predominantly in Kupffer cells for both formulations due to size restrictions for passing through liver sinusoids.[21] The non-biodegradable PS-iFNP-NCs accumulate in the liver and show no signs of further clearance. While the biodegradable PLA-iFNP-NCs also clear to the liver, observation of signal in the gut may indicate degradation in the liver, followed by the release of either the copper chelate or larger NC fragments to the gut by biliary clearance.[22,23]

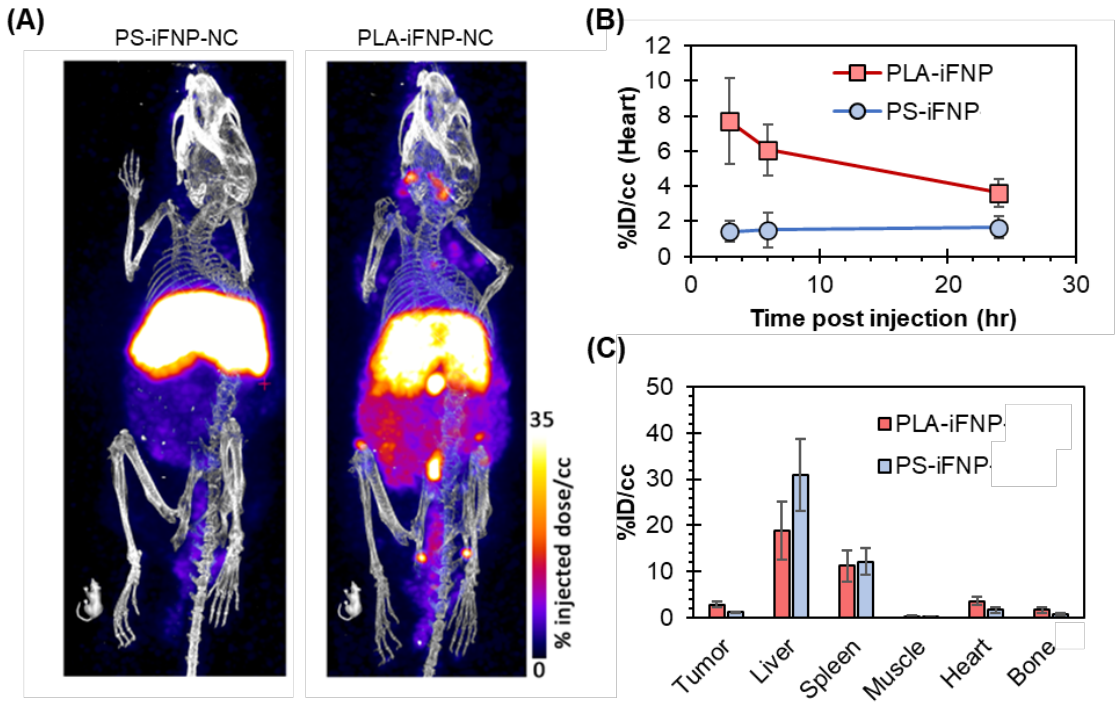

Figure 3: (A) Maximum intensity projections of the formulations tested in vivo at 24 hours. (B) Cardiac signal (%ID/cc) was used as a surrogate for blood circulation time. As expected, the unstable PS-iFNP-NC was rapidly cleared from circulation by 3 hours. (C) Tissue biodistribution at 24 hours for the formulations (%ID/cc). The signal in the gut and lymphatics was not quantified.

Kinetic analysis of the cardiac signal (%ID/cc) as a surrogate of vascular circulation confirmed the extended circulation time of PLA-iFNP-NCs, which decreased by about half from 3 hours to 24 hours (Figure 3B). These clearance kinetics corresponds closely to those we previously observed for PEG-coated solid NCs produced by FNP.[24] While the previous study directly measured radiometric values of NCs in blood using ^{125}I, the decrease in NC concentration was also approximately 50% between 3 and 24 hours (see Figures 4 and 5 in reference 24). In contrast, the PS-iFNP-PEG formulation was rapidly depleted from circulation by 3 hours (Fig. 3B).

Tumor tissue sections were characterized for vascular perfusion, macrophage distribution, and ^{64}Cu autoradiography (Figure 4, Figure S10). The ^{64}Cu signal is not strongly correlated with either high or low vascular perfusion or macrophage localization regions. The combination of high macrophage density plus the relatively low spatial resolution of the digital autoradiography technique is insufficient to fully resolve whether the iFNP-NC distribution is governed explicitly by accumulation in tumor macrophages. It appears that cellular or vascular density properties and potentially interstitial pressure may have influenced the distribution, but these alone do not account for the observed iFNP-NC localization.

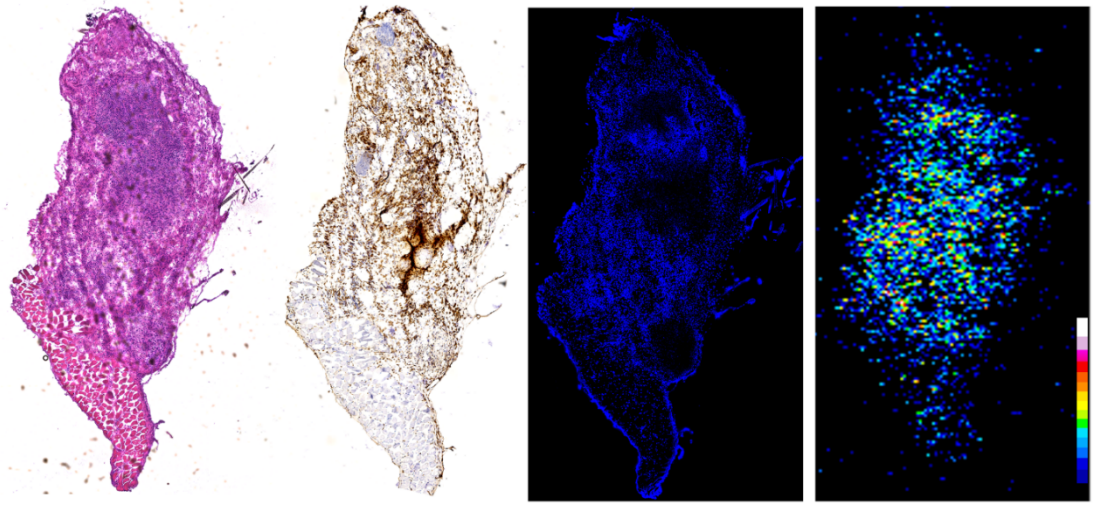

Figure 4: Spatially-registered tumor sections from PS-iFNP-NC treatment. From left to right: H&E staining, immunohistochemistry staining for F4/80 mouse macrophage, vascular perfusion with Hoechst 33342, and 64Cu autoradiography.

Formulation effects on iFNP-NC surface properties and stability

This unexpected difference in clearance behavior required an explanation. Monitoring of size and zeta potential (surface charge) of the iFNP-NCs in the physiologically relevant RPMI media without fetal bovine serum supplement showed an instability in the zeta potential for the PS-iFNP-NCs (Fig. 5A). The PLA-iFNP-NC zeta potential remained constant at -5 mV. In contrast, the PS-iFNP-NCs showed a decrease in zeta potential from -5 mV to -15 mV over 24 hours. This behavior was not observed for PS-iFNP-NCs when ‘762 was not included in the formulation (SI Figure S13-S15 and Table S1). Incorporation of the ‘762 dye and vitamin E into the PS shell resulted in instability wherein the negatively charged acrylic acid groups became exposed on the NC surface (Figure 5B). For PLA-iFNP-NC, the ‘762 dye was found to be in an aggregated state (SI Figure S6), reflecting phase separation from the PLA shell that limited intermixing with the PLA chains and may have promoted PLA shell stability.

The ability of negatively charged NCs to strongly interact with macrophages and dendritic cells via scavenger receptors is well documented. The development of a negative charge *in vivo* would be expected to drive uptake by macrophages in the liver and spleen, which typically produces the rapid clearance that we observed for PS-iFNP-NCs.[18,19]

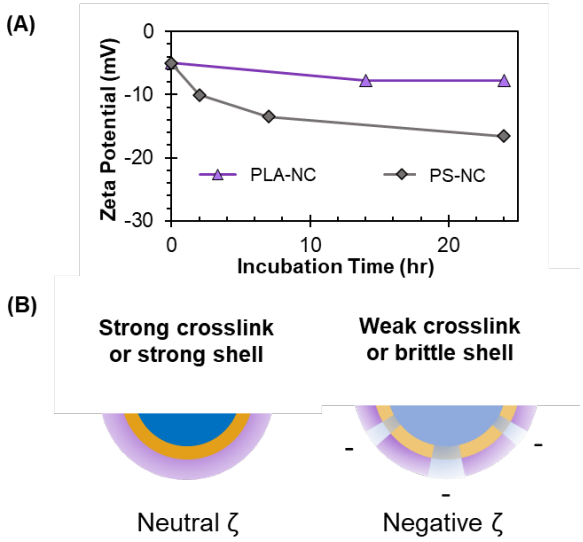

Figure 5: (A) Surface charge as measured by zeta potential during incubation in RPMI media. (B) Schematic representation of structure instability producing the negative surface charge from exposure of the anionic iFNP core.

Cell interactions provide further insight beyond surface charge

Zeta potential measurements are a population-averaged surface property that does not directly predict cell interactions or *in vivo* biodistribution. Given the promising performance of PLA-iFNP-NCs, we wanted to confirm that the measured neutral PEG surface translated into reduced cell interactions *in vitro*. Notably, iFNP-NCs did not exhibit any detectable cell lysis in a standard hemolysis assay (Figure S10). We also screened interactions of fluorescently labeled NCs after 10-minute and 24-hour incubation times with HepG2 (human hepatocyte), HEK293T (embryonic kidney), and Tib-67 (mouse-transformed monocyte) cultures using flow cytometry.

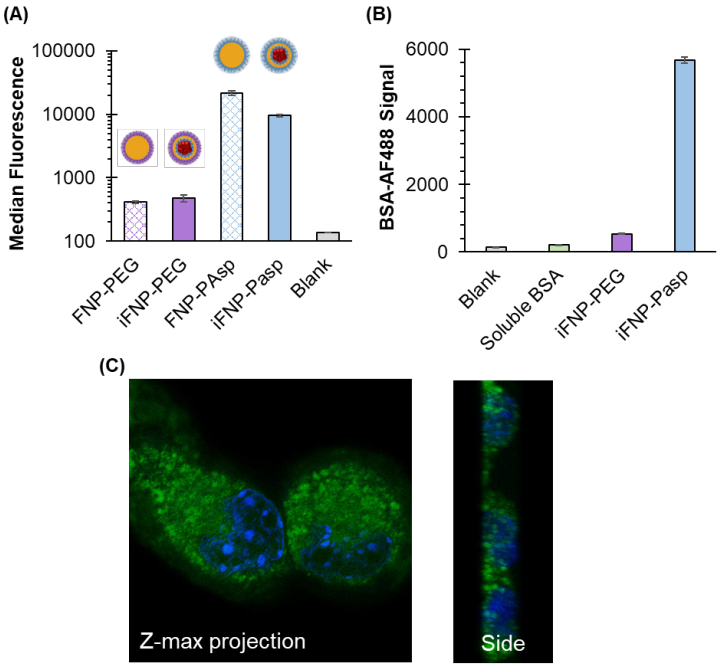

Figure 6: (A) Mean fluorescence intensity after 24 hours of incubation with the Tib-67 cell line was measured for FNP-NC and iFNP-NCs. The bar represents the average triplicates, and error bars are the standard error. (B) Fluorescent BSA was incubated with Tib-67 cells for 24 hours either as a soluble species or encapsulated by iFNP. Average of triplicates. (C) Representative confocal image of iFNP-NC after 24-hour incubation with Tib-67 cell.

To monitor iFNP-NCs, we end-labeled PLA_{15k}-*b*-$PAsp_{2k}$ with Alexa Fluor 488 to create fluorescent iFNP-NCs.

This affords NCs with polymer-linked fluorophore located in the core. As a positive control for core instability, we prepared negatively charged, PAsp-coated iFNP-NCs. As additional controls, we also prepared NCs with a purely hydrophobic PLA core by FNP using either a neutral (FNP-PEG) or negative (FNP-PAsp) surface, incorporating the fluorophore DiO for detection.

Across the three cell types, we observed that iFNP-NCs recapitulated the behavior of the analogous FNP-NC (Fig. 6A and SI Figure S12). NCs with a PEG coating resulted in limited cell interactions in all cell types; whereas a negative surface charge (PAsp coating) promoted interactions. Surface properties rather than the core structure (*i.e.*, FNP-NC versus iFNP-NC) dictated the extent of interactions. Regardless of charge, monocyte interactions were the most extensive among the cell types evaluated. These findings provide further confirmation that PLA-iFNP-NCs possess a stable PEG surface coating.

To confirm that our observations were independent of the model biologic encapsulated in the PLA-iFNP-NC, we repeated the uptake study using iFNP-encapsulated fluorescently tagged BSA. The lack of uptake for PEG-protected NCs was parallel to the cell-only and soluble BSA controls (Fig. 6B). PAsp-coating of the NCs enhanced the signal 100-fold over PEG coating ($P<0.001$).

The consistent behavior across different model core materials (dextran, lysozyme, BSA, and hydrophobic cores) demonstrates that the surface properties for PLA-iFNP-NCs are invariant with other biologics as encapsulated species. Confocal microscopy confirmed extensive internalization of the PAsp-coated NCs rather than simple surface binding, as indicated by punctate fluorescence throughout the cell (Figure 6C).

Discussion

The successful loading of ^{64}Cu to enable PET imaging of protein-containing-NCs with different cores and surface coronas, prepared by inverse Flash NanoPrecipitaiton (iFNP), has been demonstrated. These formulations \have then been applied to understand the *in vivo* fate of iFNP nanocarriers. iFNP is a two-step process that first involves the formation of an NC with a hydrophilic core comprising the biologic. The second step coats the NC with a biocompatible PEG layer. To enable PET imaging, a copper chelator, '762, is incorporated into the hydrophobic shell layer of the NC. The ^{64}Cu PET radionuclide is bound in the NC immediately before dosing by merely incubating the NC with ^{64}Cu. We have previously demonstrated this loading and imaging of NCs with PS + VitE-Ac cores and PEG surfaces.[13,14]

We expected that the exterior surface (corona) of the NC would determine the interactions of the iFNP-NC with the biological milieu *in vivo*. Therefore, two NCs with the same surface properties should have similar *in vivo* fates, independent of the composition of the core. Two iFNP constructs were made with the same 5kDa PEG surfaces but comprising two different hydrophobic shells: polystyrene (PS) and polylactic acid (PLA). They displayed very differently *in vivo* circulation and distribution profiles. The PS-iFNP-NCs displayed rapid clearance to the liver, while the PLA-iFNP-NCs exhibited sustained circulation with eventual liver/biliary clearance.

Our initial formulation selection work was carried out without the chelator. In that work, we identified polymer molecular weight and ionic crosslinkers that afforded stable size and zeta potential during buffer exposure (SI Table S1). We later found that when the '762 chelator was added to the iFNP-NC formulations, the stability (*i.e.,* size and zeta potential) of the PLA-iFNP-NCs was not affected. However, the inclusion of the copper chelator and tocopherol acetate (necessary for efficient copper binding within the glassy PS shell) compromised the stability of the PS-iFNP-NCs. In incubation with RPMI media at 37 °C, the zeta potential of the PS-iFNP-NCs decreased to -15 mV over 24 hrs. The PS block size (52 kDa) for the iFNP-NC is above the molecular entanglement weight for PS (19 kDa).[25] Thus, the original pure PS shell appears to have been mechanically strong, but the inclusion of tocopherol acetate and '762 compromised its ability to maintain encapsulation. The negative (−17 mV) surface potential on the PS-iFNP-NC is consistent with the anionic poly(acrylic acid) core exposed on the NC surface. A purely poly(acrylic acid) surface would have afforded a zeta poten-

tial of around −30 mV. In contrast, the data indicates partial exposure of the NC core – a mixed PEG and poly(acrylic acid) surface.

Our data showing different fates and biodistribution of the two iFNP-NCs demonstrate that surface properties determine NC fate. Anionic PS-iFNP-NCs, which result in the NC shell's destabilization and the polyacid core's exposure, are rapidly cleared without the sustained circulation expected for a PEG surface.

Conclusions

We have demonstrated PET imaging of NCs encapsulating biologics that are enabled by including the hydrophobic phthalocyanine dye ('762) into the hydrophobic shell of an iFNP NC. The structure of an iFNP NC is a hydrophilic biologic in the core, encapsulated in a hydrophobic shell. The iFNP process enables the encapsulation of RNA, peptide, protein, or soluble biologics into the core of the NC at high loading and high loading efficiency. The shell is covered in a biocompatible corona, which for this study was PEG. Two hydrophobic shells were investigated, one formed from the bilayer coating of PS block copolymers and the other from bilayers of PLA. PET imaging was achieved by simply incubating the pre-formed NC with ^{64}Cu radioisotope. The radioisotope loads quickly and quantitatively. Unexpectedly, the clearance and fate of the two NC formulations was substantially different even though both had initially been produced with identical 5K PEG coronas. The NC with the PS shell cleared rapidly to the liver, and the NC with the PLA shell was long-circulating, accumulating in the tumor and lymph nodes. The differences between the two were determined to be an instability that occurred with the PS-iFNP-NC when the chelator was added to the PS shell. The instability resulted in the PS-iFNP-NC developing a negative zeta potential and had clearance profiles similar to previous reports of negatively charged NCs. Without the added chelator in the PS shell this instability was not observed *in vitro*. The long circulation, deposition at the tumor site, and lymphatic accumulation of PLA-iFNP-NCs would indicate that the biodegradable NC may be of primary interest for oncology applications. Furthermore, the addition of hydrophobic chelator to the hydrophobic shell demonstrates that the PLA-iFNP-NC shows promise for the co-encapsulation of biologics and hydrophobic therapeutics using the iFNP process.

Conflict of interests

RKP and ME have a financial interest in Optimeos Life Sciences, which provided partial support for these studies. CEM is now employed by Optimeos and also has a financial stake. CEM and RKP are authors on patents for iFNP, which are licensed by Optimeos. Other authors have no relevant financial or non-financial interests to disclose. For signed statements contact the journal office editor@precision-nanomedicine.com.

Funding:

This work was supported by the PhRMA Foundation Predoctoral Fellowship in Pharmaceutics and by Optimeos Life Sciences. RKP was also supported by the Bill and Melinda Gates Foundation (BMGF, OPP1150755).

Acknowledgments

The authors wish to acknowledge Bob Mach for using his laboratory space during the ^{64}Cu chelation experiments.

Refer to this article as Chester E. Markwalter CE, Leon Z. Wang LZ, Ola M Sharaf OM, Prashanth Padakanti P, Mark Esposito M, Brian K. Wilson BK, Eric Blankemeyer E, Sean D. Carlin SD, Abass Alavi A, Prud'homme RK, Polymeric nanocarriers co-encapsulating PET probes and protein therapeutics, *Precis. Nanomed.* 2022, 5(4):994-1006, https://doi.org/10.33218/001c.xxxxx

References

1. Markwalter CE, Pagels RF, Wilson BK, Ristroph KD, Prud'homme RK. Flash NanoPrecipitation for the Encapsulation of Hydrophobic and Hydrophilic Compounds in Polymeric Nanoparticles. *JoVE.* 2019(143):e58757.
2. Markwalter CE, Prud'homme RK. Inverse Flash NanoPrecipitation for Biologics Encapsulation: Understanding Process Losses via an Extraction Protocol. *Control of Amphiphile Self-Assembling at the Molecular Level: Supra-Molecular Assemblies with Tuned Physicochemical Properties for Delivery Applications.* Vol 1271: American Chemical Society; 2017:275-296.
3. Markwalter CE, Prud'homme RK. Design of a Small-Scale Multi-Inlet Vortex Mixer for Scalable Nanoparticle Production and Application to the Encapsulation of Biologics by Inverse Flash NanoPrecipitation. *J Pharm Sci.* 2018;107(9):2465-2471.
4. Pagels RF, Prud'homme RK. Inverse Flash NanoPrecipitation for Biologics Encapsulation: Nanoparticle Formation and Ionic Stabilization in Organic Solvents. *Control of Amphiphile Self-Assembling at the Molecular Level: Supra-Molecular Assemblies with Tuned Physicochemical Properties for Delivery Applications.* Vol 1271: American Chemical Society; 2017:249-274.
5. Pagels RF, Prud'homme RK. Polymeric nanoparticles and microparticles for the delivery of peptides, biologics, and soluble therapeutics. *J Control Release.* 2015;219:519-535.
6. Markwalter CE, Pagels RF, Hejazi AN, Gordon AGR, Thompson AL, Prud'homme RK. Polymeric nanocarrier formulations of biologics using inverse Flash NanoPrecipitation. *AAPS J.* 2020.
7. Markwalter CE, Pagels RF, Hejazi AN, et al. Sustained release of peptides and proteins from polymeric nanocarriers produced by inverse Flash NanoPrecipitation. *J Control Release.* 2021;334:11-20.
8. D'Addio SM, Prud'homme RK. Controlling drug nanoparticle formation by rapid precipitation. *Adv Drug Deliv Rev.* 2011;63(6):417-426.
9. Johnson BK, Prud'homme RK. Flash NanoPrecipitation of Organic Actives and Block Copolymers using a Confined Impinging Jets Mixer. *Aust J Chem.* 2003;56:1021-1024.
10. Johnson BK, Prud'homme RK. Mechanism for Rapid Self-Assembly of Block Copolymer Nanoparticles. *Phys Rev Lett.* 2003;91(11):118302-118302.
11. Saad WS, Prud'homme RK. Principles of nanoparticle formation by flash nanoprecipitation. *Nano Today.* 2016;11(2):212-227.
12. Feng J, Markwalter CE, Tian C, Armstrong M, Prud'homme RK. Translational formulation of nanoparticle therapeutics from laboratory discovery to clinical scale. *J Transl Med.* 2019;17(200):200-200.
13. Wang LZ, Lim TL, Padakanti PK, et al. Kinetics of Nanoparticle Radiolabeling of Metalloporphyrin with 64Cu for Positron Emission Tomography (PET) Imaging. *Industrial & Engineering Chemistry Research.* 2020.
14. Lu HD, Wang LZ, Wilson BK, et al. Copper Loading of Preformed Nanoparticles for PET-Imaging Applications. *ACS App Mat & Int.* 2018;10(4):3191-3199.
15. Lee SH, Soh H, Chung JH, et al. Feasibility of real-time in vivo 89Zr-DFO-labeled CAR T-cell trafficking using PET imaging. *PLoS One.* 2020;15(1):e0223814.
16. Hennrich U, Benešová M. [68Ga] Ga-DOTA-TOC: the first FDA-approved 68Ga-radiopharmaceutical for PET imaging. *Pharmaceuticals.* 2020;13(3):38.
17. Colino CI, Lanao JM, Gutierrez-Millan C. Targeting of Hepatic Macrophages by Therapeutic Nanoparticles. *Front Immunol.* 2020;11(March):1-17.
18. Ngo W, Ahmed S, Blackadar C, et al. Why nanoparticles prefer liver macrophage cell uptake in vivo. *Adv Drug Deliv Rev.* 2022; 185:114238-114238.
19. Getts DR, Shea LD, Miller SD, King NJCC. Harnessing nanoparticles for immune modulation. *Trends Immunol.* 2015;36(7):419-427.
20. Kalbasi A, Komar C, Tooker GM, et al. Tumor-Derived CCL2 Mediates Resistance to Radiotherapy in Pancreatic Ductal Adenocarcinoma. *Clin Cancer Res.* 2017;23(1):137-148.
21. Poon W, Zhang YN, Ouyang B, et al. Elimination Pathways of Nanoparticles. *ACS Nano.* 2019;13(5):5785-5798.
22. Dowling RH. The enterohepatic circulation. *Gastroenterology.* 1972;62(1):122-140.

23. Okour M, Brundage RC. Modeling enterohepatic circulation. *Current Pharmacology Reports.* 2017;3(5):301-313.
24. Tang C, Edelstein J, Mikitsh JL, et al. Biodistribution and fate of core-labeled I-125 polymeric nanocarriers prepared by Flash NanoPrecipitation (FNP). *Journal of Materials Chemistry B.* 2016;4(14):2428-2434.
25. Herman M. Styrene polymers. *Encyclopedia of Polymer Science and Technology.* Vol 4: Wiley & Sons; 1938:247-336.